Nuclear Materials and Energy 12 (2017) 648–654

Contents lists available at ScienceDirect

Nuclear Materials and Energy

journal homepage: www.elsevier.com/locate/nme

Deuterium retention in RAFM steels after high fluence plasma exposure

Y. Martynova*, S. Möller, M. Rasiński, D. Matveev, M. Freisinger, K. Kiss, A. Kreter, B. Unterberg, S. Brezinsek, Ch. Linsmeier

Forschungszentrum Jülich GmbH, Institut für Energie- und Klimaforschung – Plasmaphysik, Jülich 52425, Germany

ARTICLE INFO

Article history:
Received 31 July 2016
Revised 29 April 2017
Accepted 30 May 2017
Available online 10 June 2017

Keywords:
EUROFER
RAFM
Deuterium
Retention
High fluence
Desorption

ABSTRACT

Deuterium retention and detrapping behavior in the ferritic-martensitic steels EUROFER'97 and P92 after exposure to plasma at high fluences $\geq 10^{26}$ D/m^2 was studied using thermal desorption spectroscopy (TDS), supported by nuclear reaction analysis. Low-temperature irradiation at 450 K and fluences $\geq 10^{26}$ D/m^2 with low impact energy D$^+$ / D$^+$+He$^+$ ions of 40 eV at PSI-2 resulted in a deuterium inventory of 7–18 $\times$ 10^{19} D/m^2 predominantly at depths $\geq$8.6 µm. Helium admixture led to a reduction of total D retention in both steels, irrespective of surface erosion and composition. The deuterium spectra of both steels displayed one D_2 desorption peak at $\sim$ 540–570 K and HD maxima at 540–590, 700–730 and 900–930 K. It is suggested that deuterium is mostly retained in the bulk of steel material on interfaces of carbide precipitates and on grain boundaries.

Introduction

In the last few decades, special steel grades have been developed on a pilot plant scale to fulfill strict long-term safety and environmental requirements for wall materials in controlled thermonuclear fusion in tokamak devices. These are reduced-activation ferritic-martensitic (RAFM) steels with about 8–11 wt.% chromium Cr and ppm low impurity traces, to accommodate the higher neutron energy in fusion reactors [1–6]. RAFM steels are proposed as structural materials for fusion reactors due to their good mechanical, corrosion and degradation properties, which were studied under realistic conditions, close to those of ITER and DEMO reactors [7,8]. It is known that hydrogen incorporation into the bulk alloy material significantly deteriorates the mechanical properties of steels [9–12]. Inventory control of hydrogen isotopes (especially radioactive tritium) in thermonuclear fusion reactor walls ensures safe operation and strongly influences the choice of plasma-facing materials (PFM) [13]. Later, the use of RAFM steels as PFM for the first wall as an alternative to tungsten (W), which was suggested for extreme conditions, is considered in recessed areas with lower heat, ion and neutron loads [14].

Among several candidate RAFM steels, the European grade EUROFER'97 was proposed for full code qualification to be used in the EU's test blanket modules for ITER on the basis of its test performance [15]. Besides low traces of impurity elements and beneficial alloying additives, EUROFER'97 contains 1.06 wt.% tungsten (W), which as a heavy element is believed to enrich at the surface due to preferential sputtering of lighter constituents during plasma exposure [16] (for the full elemental composition see [1]), thus reducing surface erosion. Due to the as yet limited availability of EUROFER'97, its sputtering behavior was approximated using an industrial ferritic-martensitic (FM) steel grade P92 [17], as both grades are similar with respect to major elemental components and phase structure [18].

Since the application of steel for the first reactor wall is limited to recessed areas with lower heat and plasma flux as compared to tungsten under normal operation conditions, helium concentration is considered to be an important factor which may affect hydrogen retention in the wall material. A number of studies on H (^{1}H), D (^{2}H) and T (^{3}H) isotopes in EUROFER'97, and also in comparison with other RAFM steels (F82H, RUSFER), have already been performed with electrochemically charged gas- and plasma-loaded samples [19–27]. Some of these studies demonstrated the advantageous behavior of RAFM steel EUROFER'97 in terms of hydrogen retention as compared to oxide-dispersion-strengthened (ODS) steel and W [21,22,24]. A recent detailed study by K. Yakushiji and co-workers addressed D retention dependences on temperature (500–818 K) and He admixture (0.5% in ion beam) for F82H RAFM steel at 1 $\times$ 10^{24} D$^+$/m^2 irradiation fluence [28]. In our present

* Corresponding author.
E-mail address: y.martynova@fz-juelich.de (Y. Martynova).

http://dx.doi.org/10.1016/j.nme.2017.05.005

experimental work, we examine for the first time deuterium (D) retention in RAFM steel EUROFER'97 after plasma exposure in PSI-2 [29] at high fluences $\geq 10^{26}$ D/m^2 focusing on a comparison with simultaneously exposed FM industrial P92 steel grade, tungsten (W) and iron (Fe) as reference materials. The aim of the study was to find a correlation between varying helium admixtures, the resulting surface microstructure, and deuterium retention in terms of integral values and trapping states.

Materials & methods

FM steels in this study are represented by RAFM EUROFER'97 (hereinafter EU'97) and P92 steel grades with 1.06 and 1.75 wt.% W (0.3 and 0.5 at.%; hereinafter W concentration is given in at. % as a bulk element component). High-purity polycrystalline W (99.96 wt. %, Plansee) and ARMCO pure iron Fe (99.9 wt. %) are used as reference materials. All samples had surface areas of 10×10 mm^2 exposed to the plasma and were 3.5 mm thick. Polished to a mirror-like finish ($R_a \sim 15$ nm) and outgassed at 500 °C (for steels - below austenitic transition, also Fe) / 1000 °C (W), in the linear plasma device PSI-2 samples were simultaneously subjected to D^+ and $D^+ + He^+$ plasmas (fraction of He ions of 0, 5, 10% (measured by optical spectroscopy), $T_e = 10$ eV) at surface temperatures T – 450 K, plasma fluxes of $4–6 \times 10^{21}$ $D^+ \cdot m^{-2} s^{-1}$ and impact energy of D^+ ions of 40 eV (target bias −65 V). The total ion fluences reached 1–1.6×10^{26} D^+/m^2, while the total pressure ($D_2 + He$) was kept constant in all experiments. The sample surface temperature was controlled by a type-K thermocouple and an infrared (IR) camera with InSb detector. The base pressure in the exposure chamber was below $2 \cdot 10^{-7}$ mbar.

Surface morphology, microstructural changes in the subsurface and elemental composition were investigated by scanning electron microscopy (SEM), by cross-sectioning with the focused ion beam (FIB) technique and by energy-dispersive X-ray spectroscopy (EDX), all coupled in a Carl Zeiss Crossbeam 540 apparatus. Nondestructive determination of D content up to a depth of 8.6 µm and elemental surface and bulk composition were performed by nuclear reaction analysis using 1.4 and 4.5 MeV accelerated $^3He^+$ ion beams and Rutherford backscattering spectrometry (NRA/RBS) with data evaluation by the SIMNRA program [30,31]. The apparatus had a dE/dx sensitive two-detector setup with a 10 µm foil 1.5 mm in thickness and 15 msr for protons and a bare 0.1 mm thickness and 5 msr detector for alphas. The NRA depth profiles are evaluated in a 2-layer approximation, where the first layer represents 0 to 0.2 µm via 1.4 MeV $^3He^+$ (in W) and the second layer represents 0.2 µm to the final measurement depth via 4.5 MeV $^3He^+$ considering everything after the first resolution point. The protons from the D(^{3}He, p) ^{4}He reaction were counted energy resolved. The product energies are correlated to a depth of origin using the implementation of stopping power of SIMNRA. Due to the limits of energy resolution, straggling and counting statistics, the integration of protons was performed only for the 2 depth ranges. The resolution for the W enrichment derived from RBS is about 35 nm. The total amount of retained D (as $D_2 + HD$) was measured by thermal desorption spectroscopy (TDS) at 10^{-8} mbar base pressure in a quartz tube. Implanted D_2 and He were differentiated by a high-resolution quadrupole mass spectrometer (QMS). This QMS, Microvision-IP from MKS Instruments, with a mass range of 1–6 amu, is able to distinguish between 4.028 amu (D_2) and 4.0026 amu (He) masses. The QMS was calibrated by the standard calibration leak method for D_2, H_2, He and HD, separately for each gas (HD averaged between D_2 and H_2). The temperature during TDS runs was controlled by a type-K thermocouple placed in vacuum near the sample and a PID control unit with a heating rate of 0.2 K/s. A number of TDS experiments with spot-welded thermocouples for each type of material (both steels, Fe, W) were carried out to improve measurement accuracy, so that the temperature was registered directly at the sample surface. Later, all the temperature curves of the 'vacuum' thermocouples were replaced by the spot-welded temperature curves as this provides more accurate temperature monitoring. Desorption rates and integral values are given in D atoms ($D \cdot m^{-2} s^{-1}$ and D/m^2, respectively). The time gap between exposures and measurements was more than one week.

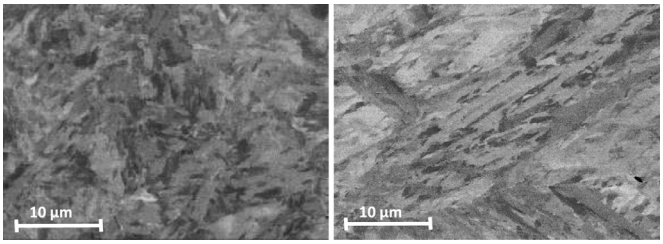

Fig. 1. SEM images of original EUROFER'97 (left) and P92 (right) steel surfaces (at 5 kV voltage).

The original surface morphology of the steel samples is shown in Fig. 1. Both steel grades exhibit a polycrystalline grain structure of ferritic-martensitic steels, which is well documented in the literature [32,33]: EU'97 samples have rather fine grains (0.5–2 µm) as compared with the strongly pronounced martensitic elongated grain geometry of P92 steel (e.g. 10 µm). Pure Fe displays large grains of about 40–50 µm size. Pure W has a polycrystalline structure with grains oriented perpendicular to the surface.

Results & discussion

As documented by SEM, after all plasma exposures had been completed the surfaces of both steels and also the iron samples demonstrated a similar porous structure (see Figs. 2 and 3). The introduction of helium by mixed exposure (with 5 and 10% He) to deuterium plasma intensified the sputtering process of steel (and iron) samples (Fig. 2, bottom row and Fig. 3, left): initially smooth grain planes turned to eroded rough surfaces with straight coral-like structures (sharp grass-like in D^+-plasma, roundish in $D^+ + He^+$-plasmas). Upon exposure to high fluence plasma the W samples displayed rough surfaces (see Fig. 3, right) as a sign of sputtering. In Fig. 4, it can be seen that the grain boundaries of the steels are decorated by some protrusive entities. Their height is about 350 nm, while the average height of the main matrix profile is about 150–210 nm. As presented in Fig. 5, EDX mapping of exposed surfaces showed that on eroded steel surfaces chromium carbide precipitates (as well as tantalum and tungsten) were visible along grain boundaries.

According to RBS characterization (see Table 1), the exposed surfaces of EU'97 and P92 steels were enriched with W (up to 6 and 7.6 at. %, ~ 20-fold as compared with initial values of 0.3 and 0.5 at.% respectively, given in *Materials and Methods*) and with molybdenum (up to 5 and 12.5×10^{19} m^{-2}), and the enrichment correlated well with the increase of the He content in D plasma. The surface of the Fe samples was also covered with W (1.2 at. %) and Mo (up to 2.2×10^{19} m^2), probably coming from sputtered W sample mask and Mo anode of the plasma source, respectively. This process is unavoidable. A factor 2 in the Mo deposition on Fe and EU'97 is within typical spans for PSI-2 samples at different sample positions, probably due to slight misalignments. Influence of slight sample temperature difference due to different thermal conductivity or magnetic field is not excluded. In order to differentiate the original W in both steels (increased due to preferential sputtering) from the deposited W, the values measured for the steels and the iron samples can be subtracted.

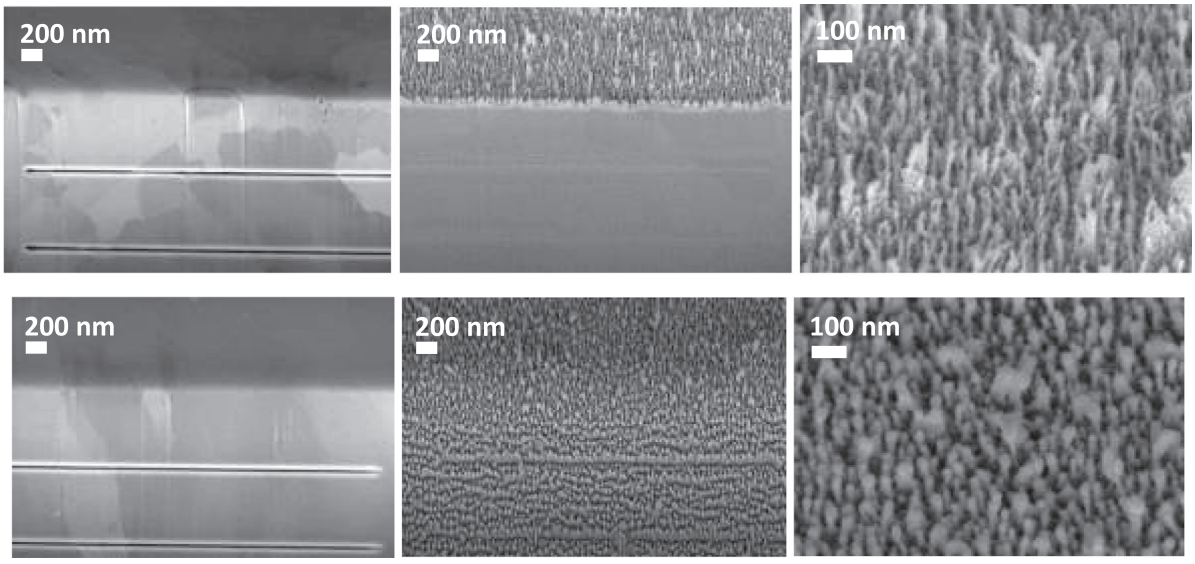

Fig. 2. SEM images of FIB cross-section before and after plasma exposure for steel EU'97 (P92: similar, not shown): upper row – exposure in pure D^+, bottom row - in $D^+ + 5\%$ He^+ . Image sequence: unexposed, exposed, exposed at doubled magnification. Horizontal notches serve as marks for visual inspection of material sputtering. Hereinafter at 3 kV voltage.

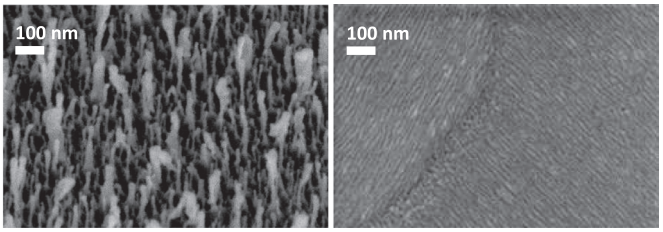

Fig. 3. SEM images of iron (left), tungsten (right) after exposure to mixed $D^+ + He^+$ plasma.

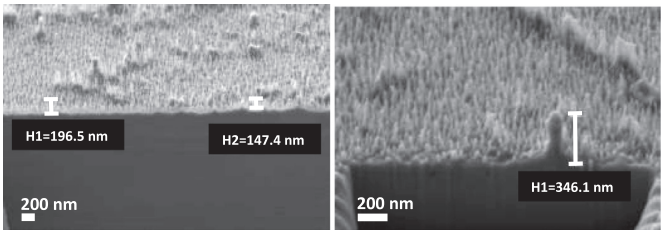

Fig. 4. Typical SEM images of eroded surface profile of P92 steel (EU'97 similar, not shown).

As documented in Table 1, NRA characterization revealed quite low values of D retention, especially in the steels and the iron samples (Σ D NRA around $2{\cdot}10^{19}$ D/m^2, error 1×10^{18} D/m^2). This observation is not in line with preferred D distribution in the near-surface region reported in [24].

According to the integration of the TDS spectra obtained, the total D retention was typically 2–5 times higher compared to the NRA data. This means that about 20–50% of the retained D is attributed to the first 8.6 μm detected by the NRA method, indicating a much deeper diffusion of D during exposure. A similar (but temperature-dependent) discrepancy between TDS and NRA measurements was recently reported in a comparative retention study for EUROFER'97 and F82H RAFM steels [23]. In our work, several trapping sites were observed in all materials. The low retention in steels can be attributed to fast deuterium diffusion and the low density of strong trapping sites as compared to W. As shown in Table 1 (column "He (TDS)"), after exposure to mixed D^++He^+ plasma, the steels and iron accumulated substantial amounts of He (in 10^{20} D/m^2 range) as compared to tungsten (in$\cdot 10^{19}$ D/m^2 range).

As presented in Fig. 6, the desorption of deuterium implanted in EU'97 samples exhibited one D_2 peak (or a number of overlapped peaks located very close to each other) at $\sim$ 560 K. This is completely in line with the available data on hydrogen retention (H) in EU'97 for electrochemically charged and plasma-charged samples where only one trapping state was registered [21,22]. A definite similarity in D (H) release was found by comparing EUROFER'97 with other RAFM steels, e.g. F82H and RUSFER [3,34,35]. In spite of outgassing before exposure, the presence of residual hydrogen, trapped in the steel from the production process, resulted in significant deuterium losses as HD, with broadened overlapped peaks (combination of TDS profiles of D_2 and H_2) at about 540–570 K, 730 K and 900 K. He admixture led to a substantial increase of the low-temperature peak in the HD profile, with a corresponding decrease of the D_2 peak and slight reduction of the integral deuterium retention ($D_2 + HD$, see Table 1). It is interesting to note that for fluence-dependent comparative studies between EUROFER'97 and F82H (with fluences $\leq 10^{25}$ D/m^2 of pure D, with biased samples) lower retention values at about 1×10^{19} D/m^2 were reported for EUROFER'97; in the study deuterium retention was measured by NRA only [23]. In our work an increase of He concentration up to 10% resulted in almost complete suppression of molecular D_2 release.

As shown on TDS profiles in Fig. 7, the release of trapped deuterium (both as D_2 and HD) from P92 steel appears similar to that from EUROFER'97 (Fig. 6). In general, similar desorption peaks were found for D_2 at $\sim$ 540 K, and for HD at about 550–590 K, 700–730 K, 840 and 930 K. With increasing He admixture, the progressive suppression of molecular D_2 release and decrease of HD formation were observed for P92 samples. However, the integral D retention (see Table 1) was on average twice as high in P92 samples at comparable He % than in EU'97 material: $8–18 \times 10^{19}$ D/m^2. To the best of our knowledge, no data are available on TDS experiments with hydrogen isotopes implanted in P92 steel by any method (gas, ions, electrochemically) in the literature, since the influence of hydrogen on industrial steels is always discussed in terms of tensile tests. Therefore, it is not possible to refer to any

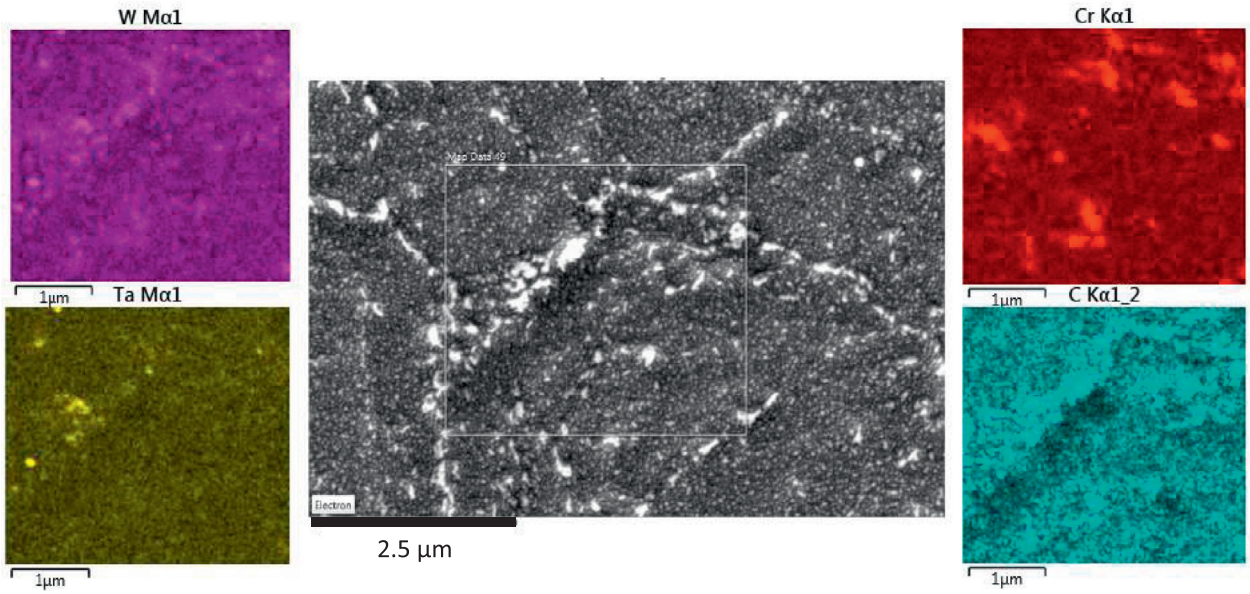

Fig. 5. Typical EDX elemental mapping of EU'97 plasma exposed surface.

Table 1
Elemental analysis by NRA/RBS and integral retention by TDS *.

Sample	He^+, vol. %	C	O	N	Mo	W [%]	D surf.	D bulk	Σ D NRA	Σ D TDS (D_2 + HD)	He (TDS)	Σ(TDS)/ Σ(NRA)
EU'97	0	12	40	20	0.7	3.5	0.8	0.35	1.15	7.01		6.1
	5	12	40	20	3	5	2.2	0.45	2.65	5.74	20.70	2.2
	10	12	40	20	5	6	2.1	0.5	2.60	6.00	16.20	2.3
P92	0	12	40	20	3	3.2	0.6	0.58	1.18	18.00		15.3
	5	12	40	20	6	5.8	1.6	0.65	2.25	10.40	13.40	4.6
	10	12	40	20	12.5	7.6	2	0.45	2.45	8.00	19.50	3.3
Fe	0	15	30	0	0.3	0.8	0.07	0	0.07	3.91		55.9
	5	15	30	0	1.1	1.2	1.2	0.08	1.28	7.58	18.40	5.9
	10	15	30	0	2	1.1	1.6	0.08	1.68	6.42	16.60	3.8
W	0	13	10	10	–	–	68	188	256.00	203.00	–	0.8
	5	13	10	10	–	–	6.5	1.8	8.30	7.39	6.25	0.9
	10	6	5	10	–	–	4.1	1.3	5.40	6.42	7.55	1.2

* all values, except W concentrations, are given in 10^{19} atoms/m^2; D_{surf}. refers to NRA analysis with 1.4 MeV $^3He^+$ ion beam (depth up to about 200 nm); D_{bulk} refers to NRA analysis with 4.5 MeV $^3He^+$ ion beam (depth up to about 8.6 μm).

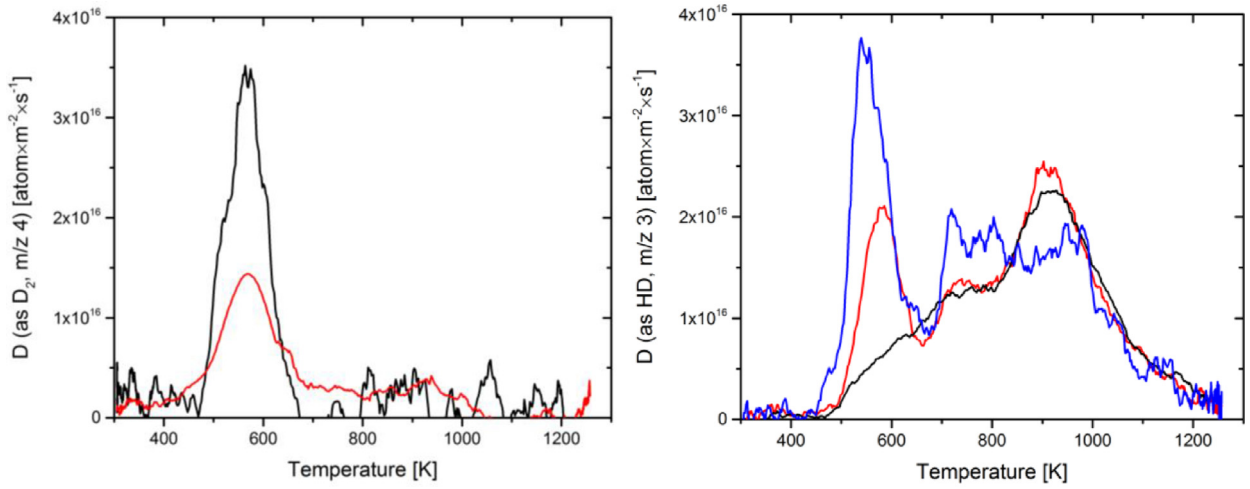

Fig. 6. Desorption profiles of D_2 (m/z = 4) and HD (m/z = 3) for EUROFER'97 after plasma exposure. Color codes refer to He^+ vol. %: black – 0, red – 5, blue (only HD, D_2 below TDS detection limit) – 10. Hereinafter m/z represents a mass-to-charge ratio of the mass of the detected ion to its electrical charge. For simplicity, m/z are given as integers. (For interpretation of the references to color in this figure legend, the reader is referred to the web version of this article).

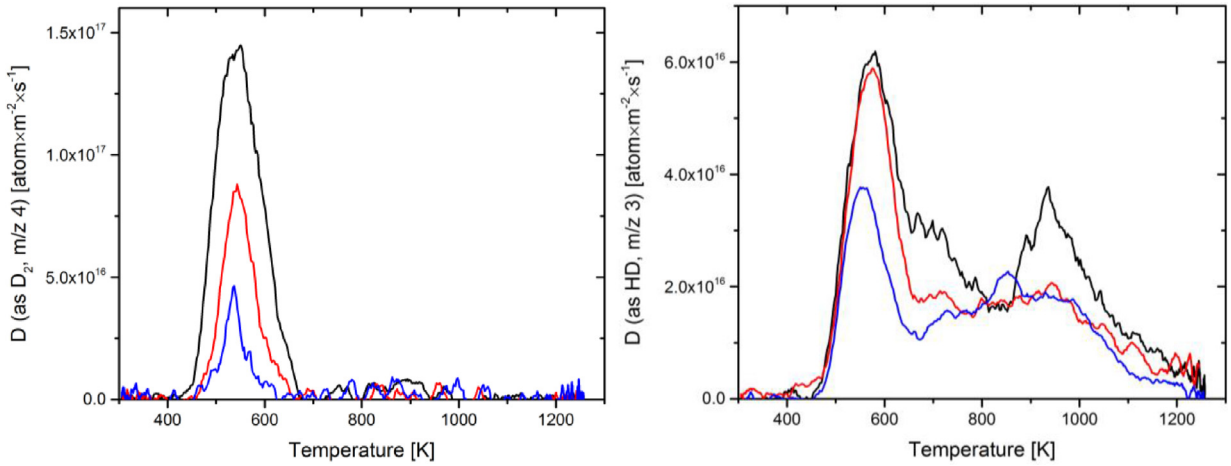

Fig. 7. Desorption profiles of D_2 (m/z = 4) and HD (m/z = 3) for P92 after plasma exposure. Color codes refer to He^+ vol. %: black – 0, red – 5, blue – 10. (For interpretation of the references to color in this figure legend, the reader is referred to the web version of this article).

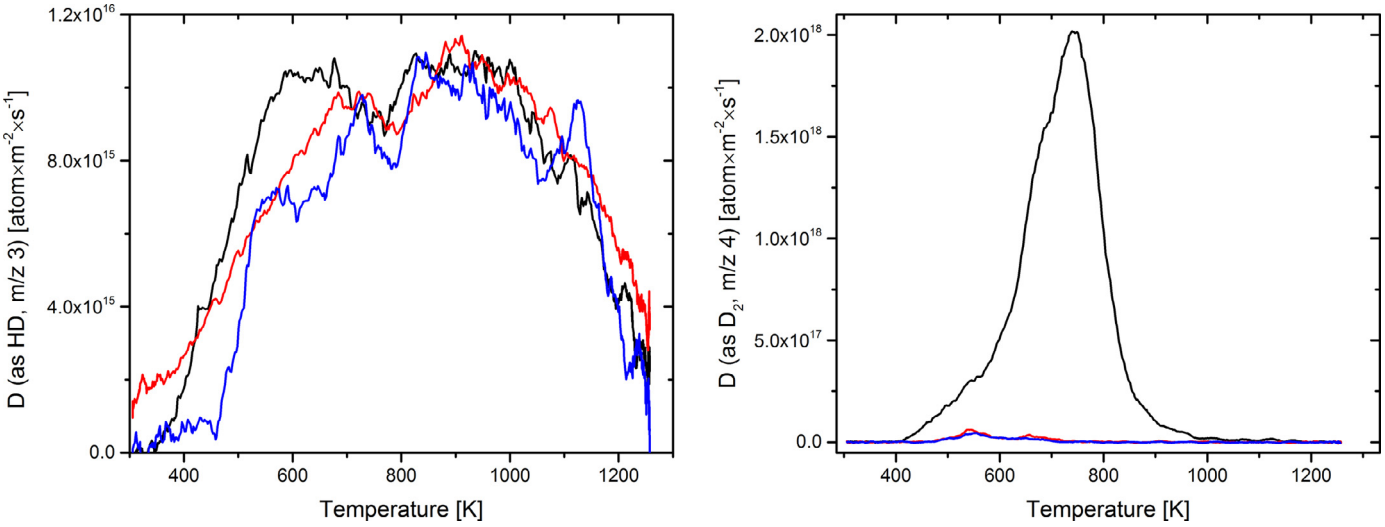

Fig. 8. Desorption profiles of HD (m/z = 3) for iron (left) and of D_2 (m/z = 4) for tungsten (right) after plasma exposure. Color codes refer to He^+ vol. %: black – 0, red – 5, blue – 10. (For interpretation of the references to color in this figure legend, the reader is referred to the web version of this article).

earlier studies on hydrogen retention in P92 steel. Higher retention and slight differences in profiles of P92 may refer to a higher concentration of some alloying elements as compared to EU'97. The decrease of the D retention with He admixture to the plasma in this study is in line with that observed for F82H RAFM steel by K. Yakushiji and co-workers [28]. They suggested that "He implanted at the near surface in RAFM steels may reduce the inward penetration of tritium".

The total D retention in the pure Fe samples is comparable with that of EU'97 samples (see Table 1): the values vary between 3.9–7.6×10^{19} D/m^2. However, detrapped D is represented mostly by HD release with no clear correlation to the He admixture, as depicted in Fig. 8 (left).

In the case of W samples, He admixture to the plasma has a much more pronounced quantitative effect on the reduction of D total retention as compared to the steel and iron samples shown in Fig. 8 (right). The integral retention in W samples after pure D exposure was two orders of magnitude higher than that of steel and iron samples: 2.0×10^{21} D/m^2. Upon the incorporation of He^+ ions, the deuterium inventory dropped to 6.4–7.4×10^{19} D/m^2. D outgassing in the form of HD was negligible for the W material. These results confirm previous investigations on PSI-2 [36].

In general, the main mechanisms and sites of hydrogen trapping in industrial and fission plant steels are described well [10–12,37]. This includes trapping on grain boundaries, point and line defects, voids, non-metallic inclusions and Laves phases. One of the trapping mechanisms in steels is the accumulation of hydrogen by metal carbides, e.g. Fe, Cr, V, Ti, Mo or mixed carbides. They are usually incorporated as fine particles in the steel microstructure along grain boundaries and form strong C–H bonds on interfaces (see overview tables with detrapping energies [38–41]). A number of studies visualized the localization of trapped hydrogen isotopes around non-metallic inclusions by tritium microautoradiography (with transmission electron microscopy (TEM)) and atom probe tomography (APT) [42–44].

Both studied steels possess a considerable amount of Cr as one of the major alloying elements. Therefore, in view of the lack of experimental data for RAFM steels and EU'97, particularly on the mechanisms and visualization of hydrogen retention, it is reasonable to apply this available knowledge. If D retention by point defects in the steel subsurface were to be the case in this work, most of the retained D should then be located within the NRA detection range (up to 8.6 µm). D trapping on Cr carbide interfaces and grain boundaries in the bulk steel material at high fluence plasma exposure could be a good hypothesis.

This hypothesis needs an additional explanation. At first, it seems that the modification of surface morphology affects the accuracy of NRA results. The NRA evaluation was made assuming a flat surface, but studied materials acquired porous surfaces after plasma exposure, with quite an inhomogeneous top layer. For D-NRA this is irrelevant, as the first resolution point is much thicker than this modified layer and cannot be resolved. The NRA errors are significant, $25\% + 0.1 \times 10^{15}$ D/cm², but still smaller than the NRA/TDS ratios derived in Table 1. Secondly, according to TDS data in Table 1, total D retention in both Fe and EU'97 was comparable. In the ion influence region (column "D surf" in Table 1), Fe and EU'97 have similar amounts of D. However, at the greater depth, a higher content of bulk carbon and carbides in the steel correlates well with the higher D bulk content resolved by NRA (column "D bulk" in Table 1). In pure iron, hydrogen is predominantly trapped at grain boundaries [45–48]. The grain size in EU' 97 is smaller than in pure iron, 0.5–2 μm and 40–50 μm, respectively (see *Materials & Methods*), which suggests the presence of more grain boundaries in the steel. However, this does not result in higher total D retention in EU'97 as compared to Fe. D trapping at grain boundaries and at carbide interfaces in FM steels represents co-existing mechanisms which do not exclude each other. Trap assignment is usually performed on the basis of detrapping activation energies and desorption peaks (see overview tables from [38–41]): lowest values are ascribed to grain boundaries, vacancies and dislocations, highest - to carbides.

Summary

The integration of desorption spectra shows that the RAFM steel EU'97 as well as P92 steel retain deuterium in the range of 10^{19} D/m^2 upon simultaneous exposure to low-temperature D^+ / D^++He^+ plasma with high fluences $\geq 10^{26}$ D/m^2. D was mostly trapped in the material bulk at depths >8.6 μm, thus demonstrating its fast diffusion in the ferritic-martensitic steels studied.

Steel surface roughening and enrichment with W due to preferential sputtering is assumed not to play a critical role in total deuterium retention after exposure to pure D^+ or mixed D^++He^+, at least at such a low energy of the incident ions as 40 eV, since implanted deuterium penetrated more deeply than the ion damage layer. However, it cannot be excluded that surface defects and deposits influence the recombination of D and H species to some extent during desorption.

An increase of the He content in the D plasma revealed similarities in D detrapping behavior in both EU'97 and P92 steels. He promoted D release via HD, which was formed almost exclusively, with suppression of D_2 desorption. The integral D retention in EU'97 decreased moderately upon He admixture, while for P92 D retention dropped more than twice as much. The D spectra of both steels displayed one D_2 desorption peak and at least three HD maxima. High peak values together with an analysis of common mechanisms of hydrogen retention in steels allow us to assume that the grain boundaries and interfaces of Cr carbides may serve as D trapping sites. In the case of a lack of EU'97 material, it seems reasonable to further model the behavior of this material by the exposure of P92 steel. At exposure to mixed D^++He^+, D retention in W takes place in the near-surface layer and is only formally comparable with that of FM steels.

Acknowledgment

This work was carried out within the framework of the EUROfusion Consortium and received funding from the Euratom research and training programme 2014–2018 under grant agreement No 633053. The views and opinions expressed herein do not necessarily reflect those of the European Commission.

References

[1] R. Lindau, et al., Present development status of EUROFER and ODS-EUROFER for application in blanket concepts, Fusion Eng, Des 75–79 (2005) 989–996.
[2] K. Shiba, H. Tanigawa, T. Hirose, T. Nakata, Development of the toughness-improved reduced-activation F82H steel for DEMO reactor, Fus. Sci. Technol. 62 (2012) 145–149.
[3] A.V. Golubeva, et al., Hydrogen interaction with the low activation ferritic–martensitic steel EK-181 (Rusfer), J. Nucl. Mat. 438 (2013) S983–S987.
[4] Q. Huang, Development status of CLAM steel for fusion application, J. Nucl. Mat. 455 (2014) 649–654.
[5] S.J. Noh, S.K. Lee, W.J. Byeon, Y.B. Chun, Y.H. Jeong, Transport of hydrogen and deuterium in the reduced activation martensitic steel ARAA, Fus. Eng. Des. 89 (2014) 2726–2731.
[6] T. Jaykumar, et al., Reduced activation ferritic martensitic steel and fabrication technologies for the Indian test blanket module in ITER, Fus. Sci. Technol. 65 (2014) 171–185.
[7] N. Baluc, R. Schäublin, P. Spätig, M. Victoria, On the potentiality of using ferritic/martensitic steels as structural materials for fusion reactors, Nucl. Fus. 44 (2004) 56–61.
[8] R.J. Kurtz, et al., Recent progress toward development of reduced activation ferritic/martensitic steels for fusion structural applications, J. Nucl. Mater. 386-388 (2009) 411–417.
[9] K. Splichal, J. Berka, J. Burda, M. Zmitko, Fracture toughness of the hydrogen charged EUROFER 97 RAFM steel at room temperature and 120°C, J. Nucl. Mater. 392 (2009) 125–132.
[10] R.L. Klueh, D.R. Harries, High-Chromium Ferritic and Martensitic Steels for Nuclear Applications, American Society for Testing and Materials, West Conshohocken, Pennsylvania, 2001.
[11] R.P. Gangloff, B.P. Somerday, Gaseous Hydrogen Embrittlement of Materials in Energy Technologies; v.2: Mechanisms, Modelling and Future Developments, first ed., Woodhead Publishing Limited, Cambridge, United Kingdom, 2012.
[12] M. Nagumo, Fundamentals of Hydrogen Embrittlement, first ed., Springer, 2016 e-book.
[13] J. Roth, Tritium inventory in ITER plasma-facing materials and tritium removal procedures, Plasma Phys. Control. Fus. 50 (2008) 103001.
[14] J. Roth, K. Sugiyama, V. Alimov, T. Höschen, M. Baldwin, R. Doerner, EUROFER as wall material: reduced sputtering yields due to W surface enrichment, J. Nucl. Mater. 454 (2014) 1–6.
[15] F. Tavassoli, Eurofer steel, development to full code qualification, Procedia Eng. 55 (2013) 300–308.
[16] M. Rasinski, et al., Morphology and composition of Fe-W coatings after deuterium plasma exposure as a model system for RAFM steels, Phys, Scripta T167 (2016) 014013.
[17] I. Zammuto, L. Giannone, A. Houben, A. Herrmann, A. Kallenbach, Long term project in ASDEX upgrade: implementation of ferritic steel as in vessel wall, Fus. Eng. Des. 98–99 (2015) 1419–1422.
[18] F. Abe, T. Horiuchi, M. Taneike, K. Sawada, Stabilization of martensitic microstructure in advanced 9Cr steel during creep at high temperature, Mater. Sci. Eng. A 378 (2004) 299–303.
[19] G.A. Esteban, A. Peña, I. Urra, F. Legarda, B. Riccardi, Hydrogen transport and trapping in EUROFER'97, J. Nucl. Mater. 367–370 (2007) 473–477.
[20] G.A. Esteban, A. Peña, F. Legarda, R. Lindau, Hydrogen transport and trapping in ODS-EUROFER, Fus. Eng. Des. 82 (2007) 2634–2640.
[21] E. Malitckii, Y. Yagodzinskyy, H. Hänninen, Hydrogen uptake from plasma and its effect on EUROFER 97 and ODS-EUROFER steels at elevated temperatures, Fus. Eng. Des. 98–99 (2015) 2025–2029.
[22] E. Malitckii, Comparative study of hydrogen uptake and diffusion in ODS steels, Fus. Eng. Des. 88 (2013) 2607–2610.
[23] N. Ashikawa, K. Sugiyama, A. Manhard, M. Balden, W. Jacob, Effects of surface modifications on deuterium retention in F82H and EUROFER exposed to low-energy deuterium plasmas, Fus. Eng. Des. 112 (2016) 236–239.
[24] O.V. Ogorodnikova, K. Sugiyama, Effect of radiation-induced damage on deuterium retention in tungsten, tungsten coatings and Eurofer, J. Nucl. Mater. 442 (2013) 518–527.
[25] Y. Hatano, Tritium retention in reduced-activation Ferritic/Martensitic steels, Fus. Sci. Technol. 67 (2015) 361–364.
[26] V.Kh. Alimov, et al., Surface modification and sputtering erosion of reduced activation ferritic martensitic steel F82H exposed to low-energy, high flux deuterium plasma, Nucl. Mater. Ener. 7 (2016) 25–32.
[27] V.Kh. Alimov, et al., Surface modification and deuterium retention in reduced activation ferritic martensitic steels exposed to low-energy, high flux D plasma and D_2 gas, Phys. Scripta T159 (2014) 014049.
[28] K. Yakushiji, H.T. Lee, M. Oya, Y. Hamaji, K. Ibano, Y. Ueda, Influence of helium on deuterium retention in reduced activation ferritic martensitic steel (F82H) under simultaneous deuterium and helium irradiation, Phys, Scripta T167 (2016) 014067.
[29] A. Kreter, et al., Linear plasma device PSI-2 for plasma-material interaction studies, Fus. Sci. Technol. 68 (2015) 8–14.
[30] M. Mayer, Improved physics in SIMNRA 7, Nucl. Instr. Meth. B 332 (2014) 176–180.
[31] V.Kh. Alimov, M. Mayer, J. Roth, Differential cross-section of the D(^{3}He, p)^{4}He nuclear reaction and depth profiling of deuterium up to large depths, Nucl. Instr. Meth. Phys. Res. B 234 (2005) 169–175.

[32] M. Eddahbi, M.A. Monge, T. Leguey, P. Fernández, R. Pareja, Texture and mechanical properties of EUROFER 97 steel processed by ECAP, Mater. Sci. Eng. A 528 (2011) 5927–5934.
[33] L. Xu, et al., Precipitation behavior and martensite lath coarsening during tempering of T/P92 ferritic heat-resistant steel, Int. J. Min. Met. Mater. 21 (2014) 438–447.
[34] D. Hamaguchi, et al., The trapping behavior of deuterium in F82H ferritic/martensitic steel, J. Nucl. Mater. 386–388 (2009) 375–378.
[35] T. Ito, et al., Deuterium retention in F82H after low energy hydrogen ion irradiation, J. Nucl. Mater. 417 (2011) 1147–1149.
[36] M. Reinhart, et al., Influence of plasma impurities on the deuterium retention in tungsten exposed in the linear plasma generator PSI-2, J. Nucl. Mater. 463 (2015) 1021–1024.
[37] P. Novak, R. Yuan, B.P. Somerday, P. Sofronis, R.O. Ritchie, A statistical, physical-based, micro-mechanical model of hydrogen-induced intergranular fracture in steel, J. Mech. Phys. Solids 58 (2010) 206–226.
[38] K. Bergers, E. Camisão de Souza, I. Thomas, N. Mabho, J. Flock, Determination of hydrogen in steel by thermal desorption mass spectrometry, Steel Res. Int., 81 (2010) 499–507.
[39] M. Koyama, H. Springer, S.V. Merzlikin, K. Tsuzaki, E. Akiyama, D. Raabe, Hydrogen embrittlement associated with strain localization in a precipitation-hardened Fe–Mn–Al–C light weight austenitic steel, Int. J. Hydrogen Energy. 39 (2014) 4634–4646.
[40] S. Frappart, X. Feaugas, J. Creus, F. Thebault, L. Delattre, H. Marchebois, Study of the hydrogen diffusion and segregation into Fe–C–Mo martensitic HSLA steel using electrochemical permeation test, J. Phys. Chem. Sol. 71 (2010) 1467–1479.
[41] B.A. Szost, R.H. Vegter, P.E.J. Rivera-Díaz-del-Castillo, Metall. Mater. Trans. A 44 (2013) 4542–4550.
[42] C. Paes de Oliveira, M. Aucouturier, P. Lacombe, Hydrogen trapping in BCC Fe-Cr Alloys (7-9.4 Wt% Cr) as studied by microautoradiography — contribution of Carbon-Hydrogen interaction — consequences on hydrogen cracking, Corros 36 (1980) 53–59.
[43] T. Otsuka, et al., Observation of Hydrogen distribution around non-metallic inclusions in steels with Tritium microautoradiography, Fus. Sci. Technol. 48 (2005) 708–711.
[44] J. Takahashi, K. Kawakami, T. Tarui, Direct observation of hydrogen-trapping sites in vanadium carbide precipitation steel by atom probe tomography, Scr. Mater. 67 (2012) 213–216.
[45] K. Ono, M. Meshii, Hydrogen detrapping from grain boundaries and dislocations in high purity iron, Acta Metall. Mater. 40 (1992) 1357–1364.
[46] J.-Y. Lee, S.M. Lee, Hydrogen trapping phenomena in metals with B.C.C. and F.C.C. crystals structures by the desorption thermal analysis technique, Surf. Coat. Tech. 28 (1986) 301–314.
[47] Y.A. Du, L. Ismer, J. Rogal, T. Hickel, J. Neugebauer, R. Drautz, First-principles study on the interaction of H interstitials with grain boundaries in α- and γ-Fe, Phys. Rev. B 84 (2011) 144121.
[48] R. Matsumoto, M. Riku, S. Taketomi, N. Miyazaki, Hydrogen–grain boundary interaction in Fe, Fe–C, and Fe–N systems, Prog. Nucl. Sci. Technol. 2 (2010) 9–15.